The LISA Optical Bench: An Overview and Engineering Challenges

William Brzozowski, David Robertson, Ewan Fitzsimons,

Henry Ward, Jennifer Keogh, et al.

Published version information:

Citation: W Brzozowski et al. The LISA optical bench: an overview and engineering challenges. In Space Telescopes and Instrumentation 2022: Optical, Infrared, and Millimeter Wave, Montréal, Canada, 17-23 Jul 2022, (2021): 22.

DOI: 10.1117/12.2627465

PROCEEDINGS OF SPIE

SPIEDigitalLibrary.org/conference-proceedings-of-spie

The LISA optical bench: an overview and engineering challenges

William Brzozowski, David Robertson, Ewan Fitzsimons, Henry Ward, Jennifer Keogh, et al.

William Brzozowski, David Robertson, Ewan Fitzsimons, Henry Ward, Jennifer Keogh, Alasdair Taylor, Maria Milanova, Michael Perreur-Lloyd, Zeshan Ali, Andrew Earle, Daniel Clarkson, Robyn Sharman, Martyn Wells, Phil Parr-Burman, "The LISA optical bench: an overview and engineering challenges," Proc. SPIE 12180, Space Telescopes and Instrumentation 2022: Optical, Infrared, and Millimeter Wave, 121800O (27 August 2022); doi: 10.1117/12.2627465

SPIE.

Event: SPIE Astronomical Telescopes + Instrumentation, 2022, Montréal, Québec, Canada

The LISA Optical Bench: An Overview and Engineering Challenges

Bill Brzozowski*[a], David Robertson[b], Ewan Fitzsimons[a], Henry Ward[b], Jennifer Keough[a], Alasdair Taylor[b], Maria Milanova[a], Michael Perreur-Lloyd[b], Zeshan Ali[a], Andrew Earle[b], Daniel Clarkson[a], Robyn Sharman[a], Martyn Wells[a], Phil Parr-Burman[a]

[a]UK Astronomy Technology Centre, Royal Observatory Edinburgh, Edinburgh, UK
[b]SUPA, School of Physics and Astronomy, University of Glasgow, Glasgow, UK

ABSTRACT

This paper will present an overview of the LISA (Laser Interferometer Space Antenna) optical bench and discuss the innovative methods developed to analyse and mitigate significant engineering challenges. There are two optical benches for each of the three LISA spacecraft. The optical bench consists of numerous components which form the paths of the interferometers used to measure the displacement changes caused by gravitational waves. Given each spacecraft is separated by 2.5 million Km, a laser beam sent from one to another arrives with a significantly lower irradiance than on departure. It is in part because of this that various engineering challenges are faced by the LISA OB. This is alongside the extremely demanding nature of measuring gravitational waves at a sensitivity of pico-meters per root-Hertz.

Keywords: Gravitational waves, interferometry, stray light, LISA.

1. INTRODUCTION

Gravitational waves are very low in amplitude, with typical strains of about 10^{-21}. Strain being the ratio of the change in displacement and the starting displacement. GW150914, the first directly detected gravitational wave, had a peak gravitational wave strain of 1.0×10^{-21}.[1] With such a low strain, detection methods with unparalleled sensitivity are required. Laser interferometry can achieve this sensitivity and as such is the mechanism by which LISA will detect gravitational waves.

LISA will trail Earth in a heliocentric orbit and is formed of three spacecraft in a triangle formation with laser beams travelling between all three spacecraft[2]. The separation between each spacecraft is 2.5 million km, meaning LISA must be sensitive to relative displacements of $\text{picometers}/\sqrt{\text{Hz}}$ in order to detect gravitational waves. This interferometer arm-length is a significant increase on the arm-length of ground based gravitational wave detectors. LIGO, with an arm-length of 4km, can detect gravitational waves in the frequency range of 10 Hz to 10 kHz. Whereas LISA has a measurable frequency range of 0.1 mHz to 0.1 Hz – in part due to the increased arm-length, but also the absence of Earth-based noise signals. This opens up the possibility of detecting the gravitational waves from astrophysical events which sit outside the measurement range of ground-based detectors. For example, the in-spiral, merger and ringdown of massive black hole (MBH) binary systems; the in-spiral of extreme mass ratio binary systems i.e. a small black hole orbiting a MBH; or potentially the stochastic background of the Universe.[3]

There are three interferometers per optical bench in LISA – of which there are two optical benches per spacecraft, making six optical benches in total. Laser beams travel between the three spacecraft (sent and received via telescopes), around the optical benches and to and from the gravitational reference sensor (GRS), which houses the free-falling test mass (Figure 1-1). The optical bench is where these laser beams combine to generate interferometric signals, completing the three interferometers: the test mass, reference and science interferometers. This paper looks to give an overview of just the optical bench part of LISA - covering the details of how the different laser beams are manipulated and combined by numerous optics and mechanisms in order to achieve the extremely high sensitivity interferometry needed to detect gravitational waves. Furthermore, two engineering challenges caused by two of the most significant noise sources on LISA are to be explored: tilt-to-length (TTL) coupling and stray light.

Space Telescopes and Instrumentation 2022: Optical, Infrared, and Millimeter Wave, edited by Laura E. Coyle, Shuji Matsuura, Marshall D. Perrin, Proc. of SPIE Vol. 12180, 121800O · © 2022 SPIE · 0277-786X · doi: 10.1117/12.2627465

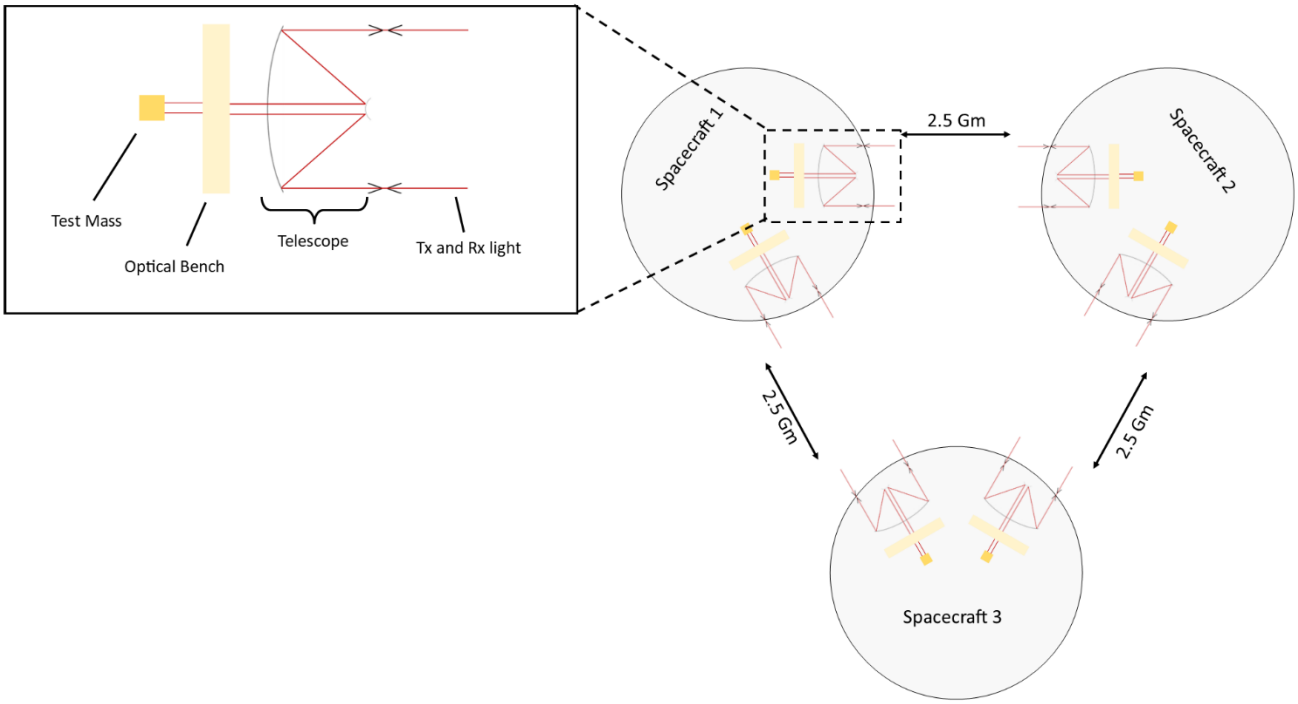

Figure 1-1: The LISA measurement scheme

*william.brzozowski@stfc.ac.uk

2. AN OVERVIEW OF THE LISA OPTICAL BENCH

The LISA optical bench has two sides: 'A' and 'B'. The A-side interfaces with the telescope, which sends and receives light to and from the far spacecraft, 2.5 million km away. The B-side interfaces with the GRS. The GRS consists of a Gold-Platinum cubic test mass, suspended in a vacuum tank. Electrostatic forces are applied to fix the position of the test mass in all degrees of freedom except one – translation along the beam axis connecting one spacecraft to another. In this axis gravity is the only external force acting on the test mass. A laser beam is reflected off this test mass and its optical path length from the optical bench is determined. For each optical bench there is an accompanying GRS. The optical path length from optical bench to test mass for each of the six optical benches (two per spacecraft), is combined with the knowledge of the optical path length between spacecraft. This gives the relative separation between test masses on separate spacecraft. In order to minimise laser frequency noise due to the arm-length mismatches between spacecraft, a technique called Time Delay Interferometry (TDI) is used when the signals are combined, see [4] for details. This is key to measuring gravitational waves, given the only significant force acting on the test masses, in the relevant axis, is gravitational force. So should a gravitational wave pass through the LISA constellation, the space-time between the test masses will expand and contract, causing a change in the phase of the light travelling between the test masses.

Figure 2-1 and Figure 2-2 show the layout of the A and B sides of the optical bench respectively. The optical bench hosts three interferometers: the science, test mass and reference interferometers. There are three laser beams used in these interferometers: Tx (transmit), Rx (receive) and the local oscillator (LO) beam. The Tx beam is shown in red, Rx is shown in green and the LO beam is shown in blue. The Tx beam is fibre fed to the optical bench from the laser and as such has the highest power, approximately 2W. This beam is transmitted to the far spacecraft via the telescope, whilst some of the Tx beam is picked off on the optical bench to be combined in the interferometers. The Rx beam is the beam received from the far spacecraft and as such is much lower power, on the order of pico-Watts. The LO beam is a sample of the Tx beam, but originating from the adjacent optical bench in the spacecraft, transferred over via a single fibre optic harness. The LO beam is brought onto the optical bench via a fibre collimator shown as 'LO beam' in Figure 2-2.

The science interferometer can be seen on the A side. A sample of the Tx beam and a sample of the Rx beams are combined at BS12 (beam splitter 12) and the interference pattern is measured at the Quadrant Photodiodes (QPD), QPD SCI-A-1, QPD SCI-A-2, QPD SCI-B-1 and QPD SCI-B-2. 'A' QPDs are considered the prime QPDs, whilst 'B' QPDs are for redundancy. Between BS12 and the QPDs, the beam passes through an imaging system, consisting of four mirrors and a beam splitter. The main purpose of the imaging system is to minimise TTL coupling and to magnify the beam down to the size of the QPD. TTL and the imaging systems are discussed in section 3.

For each prime and redundant interferometer there are two QPDs. This is for balanced detection redundancy – a scheme used to cancel stray light (ghost beams in this case) and relative intensity noise (RIN). This particular stray light and RIN arise from the 'backlink' fibre – the fibre responsible for exchanging LO beams between adjacent optical benches in the same spacecraft.

The test mass interferometer can be found on the B side of the optical bench. BS11 is the combining beam splitter for samples of the Tx beam and LO beam. However, prior to the beam combination the Tx beam has reflected off the test mass. QPD TM-A-1 and QPD TM-A-2 complete the prime test mass interferometer, whilst QPD TM-B-1 and QPD TM-B-2 complete the redundant test mass interferometer. By reflecting the Tx beam off the test mass, this interferometer determines the longitudinal position of the test mass.

The reference interferometer similarly uses a sample of the Tx and LO beams, but the Tx beam does not reflect off the GRS test mass, as is the case for the test mass interferometer. Instead the Tx beam is confined to the optical bench and is then combined at BS10 with the LO beam. QPD REF-A-1 and QPD REF-A-2 complete the prime reference interferometer, whilst QPD REF-B-1 and QPD REF-B-2 complete the redundant reference interferometer. As the reference interferometer does not interact with the GRS or the long-arm of the LISA constellation, it can act as a reference for the test mass and science interferometers, and thereby reduce noise.

Planar Silica mirrors and beam splitters are used to navigate the three beams around the optical bench in order to fit all three interferometers on the optical bench, amongst numerous components and mechanisms. This follows the same design principle as the LISA pathfinder optical bench [5]. Following on from pathfinder, the LISA optical bench will also be assembled using Hydroxide Catalysis (HC) bonding [6, 7]. See [5 and 8] for details on the metrology techniques used to assemble LISA and LISA pathfinder optics to high accuracy. An important consideration has to be made when designing the optical bench layout: that the three interferometers see an appropriately balanced number of transmissions through Silica beam splitters. This is so that the effects of changing temperature on interferometric phase are minimized. Changes in temperature can affect the interferometric phase via differential refractive index of transmissive Silica components and the different CTEs between Silica and the Zerodur optical bench.

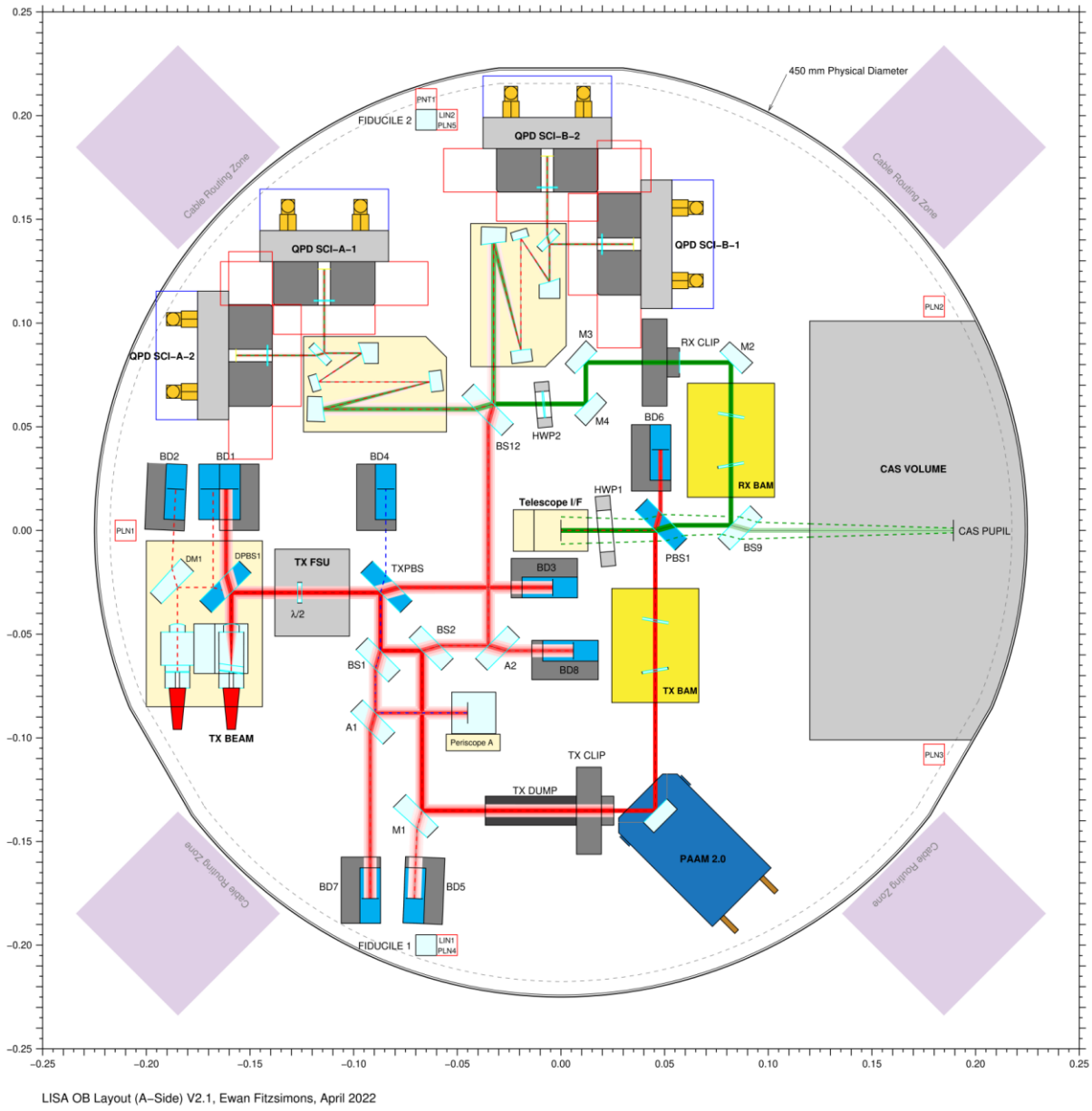

Figure 2-1: Optical layout of the A-side of the optical bench

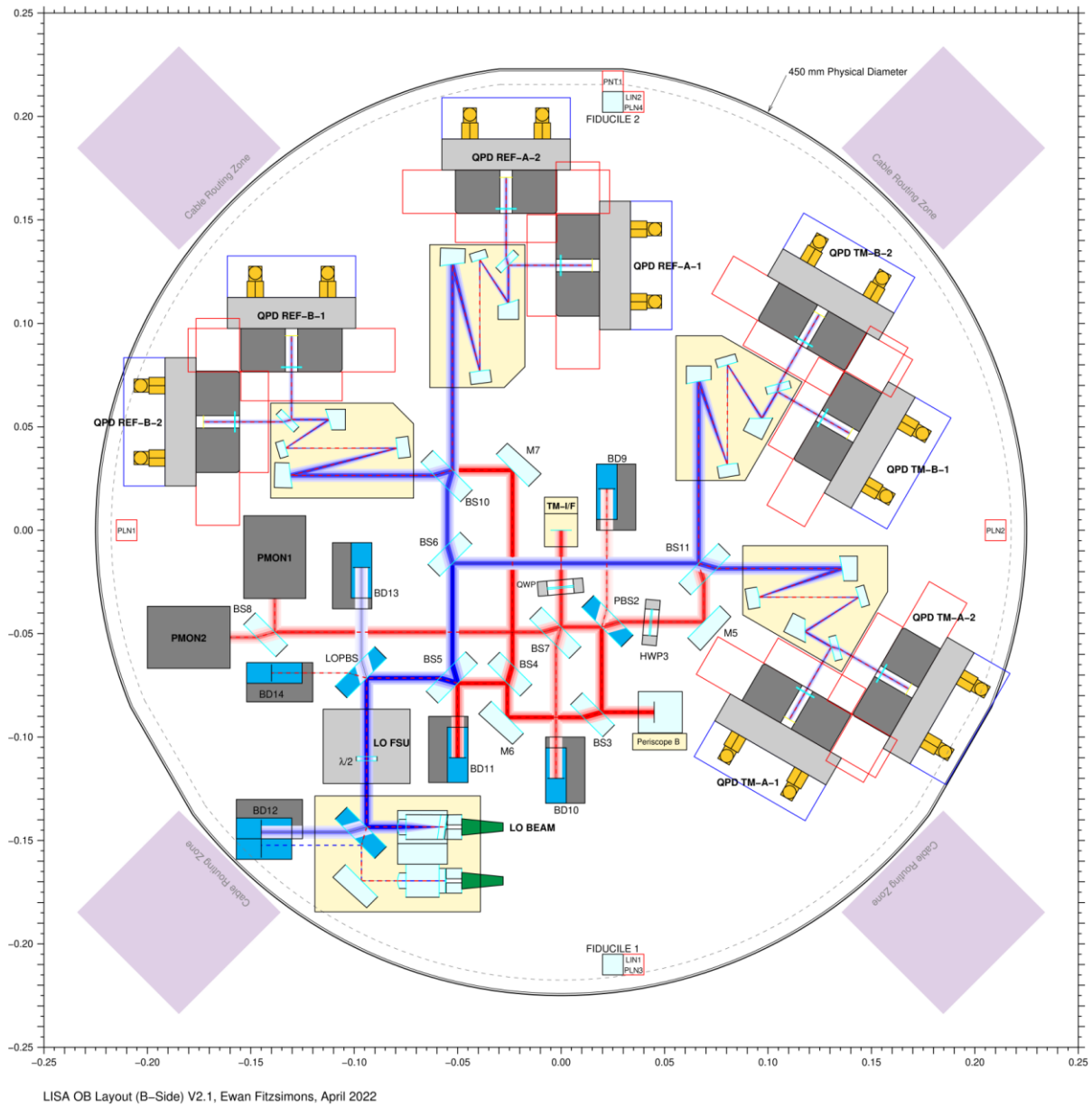

Figure 2-2: Optical layout of the B-side of the optical bench

The optical bench is visibly populated with numerous components and mechanisms. Considering the Tx path, the beam enters the optical bench on the A side via a fibre collimator – shown as 'Tx beam' in Figure 2-1. There are two fibre collimators for redundancy and a fibre switching unit (FSU), which consists of a rotatable half-wave plate, is used to correct the polarization between S-pol and P-pol, depending on which fibre collimator is being used. A polarizing beam splitter (PBS) is placed in front of the fibre collimator in order to ensure only Tx light of the correct polarization (S-pol or P-pol) is propagated onwards. The Tx light of the unneeded polarization transmits through the PBS and is dumped. The design and performance of these beam dumps, of which there are many per optical bench, is described in section 4.

BS2 is a high power beam splitter (99.5:0.5), where the higher power Tx beam is reflected towards the Point Ahead Angle Mechanism (PAAM). The PAAM is an actuated mirror sat on the pupil position and acts to change the direction of the Tx beam depending on the position of the far spacecraft that completes the interferometer arm. Just prior to the PAAM is the Tx clip and Tx beam dump. The Tx clip is positioned as close as possible to the PAAM so as to clip the Tx beam at the pupil plane. Clipping the beam here before the telescope (of fixed primary mirror size) maximises the transmission of the

Tx beam to the far spacecraft. A significant amount of light is clipped by the Tx clip, which must be heavily suppressed so as to not introduce stray light to the optical bench. The Tx beam dump achieves the necessary suppression by capturing and absorbing the clipped light from the Tx clip. Within the Tx beam dump a series of black-coated baffle vanes provide a large enough surface area to absorb the clipped light, as well as a large portion of the light which scatters off the Tx clip.

After the PAAM comes the Tx Beam Alignment Mechanism (BAM); equally an Rx BAM sits between the telescope interface and the Rx pupil plane at the Rx clip. The BAM physically aligns the Rx and Tx beam in decentre relative to the telescope. To do this, two tilted parallel plates are placed into the beam path, causing the beam to move in decentre relative to the nominal beam axis. By rotating the two plates it is possible to produce an arbitrary lateral beam offset. This adjustment is necessary such that the beam aligns to the telescope as best as possible. If the beam is off-centre relative to the telescope then a tilt in the beam at the far spacecraft is manifested. Consequently any time-varying tilts (jitter) of the local spacecraft will sweep this tilted Tx beam across the far spacecraft and cause TTL – the coupling of beam tilts into optical path length / phase changes i.e. interferometric noise. TTL is looked at in more detail in section 3, but is one of LISAs biggest noise sources that must be minimized. Hence, the BAM is the primary means of mitigating TTL in the science interferometer.

The Rx beam comes onto the optical bench via the telescope. The Rx beam profile is flat top, given the beam has diverged significantly by the time it has travelled the 2.5 million km between the spacecraft. This is compared to the Gaussian beam profile of the Tx and LO beams. The Rx BAM is then used to align the Rx beam relative to the Rx clip, such that TTL is minimised. The Rx clip, sitting at the pupil position, clips the beam to the same diameter as the Tx clip. After the beam is clipped the Rx beam then travels to the science interferometer. The Rx clip does not have an accompanying beam dump like the Tx clip because the Rx beam power is many orders of magnitude lower than the Tx beam.

Before the Rx BAM, the Rx beam is split. About 90% of the Rx beam power goes to the BAM and on to the science interferometer, whereas the remaining 10% of the Rx beam is sent to the Constellation Acquisition Sensor (CAS). The CAS is a wide field sensor and collects the Rx beam, before any interferometry is performed, in order to locate the beam sent from the far spacecraft and perform a course alignment of the LISA constellation.

3. IMAGING SYSTEMS

One of the largest noise sources for LISA is tilt-to-length coupling (TTL). TTL is fundamentally a coupling mechanism, where a time-varying tilt is introduced in the optical system which then brings about a change in optical path length [9]. Primarily, TTL is caused by misalignments and imperfections in optics. The time-varying path length change causes a longitudinal phase signal change in the interferometric signal, which is exactly the signal that a passing gravitational waves generates. Hence how TTL is a noise source for LISA, given if the time-varying tilt acts in the LISA frequency measurement band. There are numerous TTL mechanisms, depending on what part of LISA is introducing the tilt e.g. an optical bench, a spacecraft or a test mass – to name just some of the key contributors. The units of TTL are given in micron/radian or pico-meter/micro-radian i.e. length per tilt. In the context of the optical bench, and for discussion in this paper, we use ‘OB level TTL’, whereby tilts are defined in the optical bench coordinate frame. Hence, tilts are given before magnification of the telescope.

Imaging systems can be used to mitigate the effect of TTL by reducing beam tilts [9]. Specifically a pupil-to-pupil imaging system is required, as beams incident at the input pupil plane can be tilted and no extra optical path length is observed, relative to the chief ray, as the beam passes through the imaging system to the output pupil plane. This is an effective way of reducing TTL caused by time-varying tilts of the spacecraft or the test mass relative to the optical bench. Imaging systems are placed in front of the quadrant photodiodes (QPDs) for all three interferometers. As the beams used for the reference interferometer do not leave the optical bench, TTL effects are much smaller than the potential TTL that the science and test mass interferometers must suppress. However, given the optimum optical bench beam size of LISA is larger than the diameter of the QPDs, the imaging systems are also used to magnify the beams, as to prevent over-filling of the QPDs. Hence, it is still beneficial to have imaging systems placed in front of the reference interferometer QPDs.

3.1 Requirements and design constraints

There are many requirements on the design of LISA imaging systems. The magnification must be 0.4 ± 0.02 in order to not over-fill the QPD. The system should have no vignetting over a ±2.7 mrad diameter field of view, significantly larger than the performance field of view of ±500 µrad diameter. Wavefront error (WFE) degradation should be at most λ/20 RMS over the performance field of view and across a 6mm beam diameter. The TTL must be minimized with an upper limit of 13 µm/rad. All these requires are to be met under a toleranced system.

Numerous design constraints are imposed on the imaging system design. The input pupil distance is fixed and the exit pupil position had to match the QPD positions – themselves limited in location by the space constraints of the optical bench. In the interests of avoiding beam clipping, the optics are to be clear of all beams by at least 3mm. The optics are also to be kept within a few mm of the edge of the footprint allocation, given the possibility that they may be mounted to a sub-baseplate which would have a chamfered edge. Having small beam footprints on optics makes the beam susceptible to power loss and wavefront error due to surface imperfections or particulates. Hence, a minimum beam footprint size is to be aimed at of 400 µm on any imaging system optic.

3.2 Design

Both refractive and reflective imaging system designs were considered for LISA. But given that the imaging system optics need to be kept very stable (so as to avoid introducing TTL) the reflective design is preferred. This is because reflective optics can be easily mounted to the optical bench using HC bonding, which is the technique used for mounting other optics to the optical bench [6, 7]. Optics that are HC bonded to the optical bench are made from Silica, which closely matches the CTE of the Zerodur optical bench baseplate, making the optics very thermally stable. HC bonding makes a very strong bond between the optical bench and the optic by creating a layer of covalent bonds between the Zerodur and Silica. Replicating the strength and stability of a HC bond using other optic-mounting mechanisms is challenging and requires an additional technology development cycle. For example, refractive imaging systems designs made use of titanium mounts for each lens. These mounts can meet the mounting requirements (alignment, stability and strength) for the imaging system, but at the cost of extra weight and space used on the optical bench. Given there are two imaging systems per interferometer, a total of six imaging systems are needed per optical bench. Refractive designs require 3-4 lenses, meaning 18-24 lens mounts. This is to be compared to the mount-less HC bonding method used by a reflective design.

A footprint allocation was first of all determined based on what could fit onto the fixed size of the optical bench, considering all other optical bench optics, mechanisms and interface locations to the GRS and telescope. At least four mirrors were needed in order to keep a reflective imaging system design within the footprint allocation - whilst keeping the optics within the bounds of manufacturability.

A total of 18 parameters of the four-mirror imaging system were optimized against the following performance metrics: minimise TTL coupling, minimise RMS WFE over the input beam diameter and to ensure no beam footprint diameter was less than 400 µm on any optic – all whilst keeping the optics within the aforementioned physical constraints. The number of curved optics was minimised and so too was the number and magnitude of non-spherical conic surfaces. This rationale being that less curved optics and less non-spherical optics will make both the manufacture and alignment easier to achieve. To further aid the alignment of the imaging systems, where possible the tilts of optics were kept at zero. Similarly, the beam between M2 and M4 and the beam reflecting off M4 were kept as parallel to the input beam.

The TTL was minimised by measuring the maximum TTL across numerous points across the input pupil. Figure 3-1 shows the equal-area pupil sampling rings / points. At each pupil point the TTL was measured over a ±500 µrad field angle.

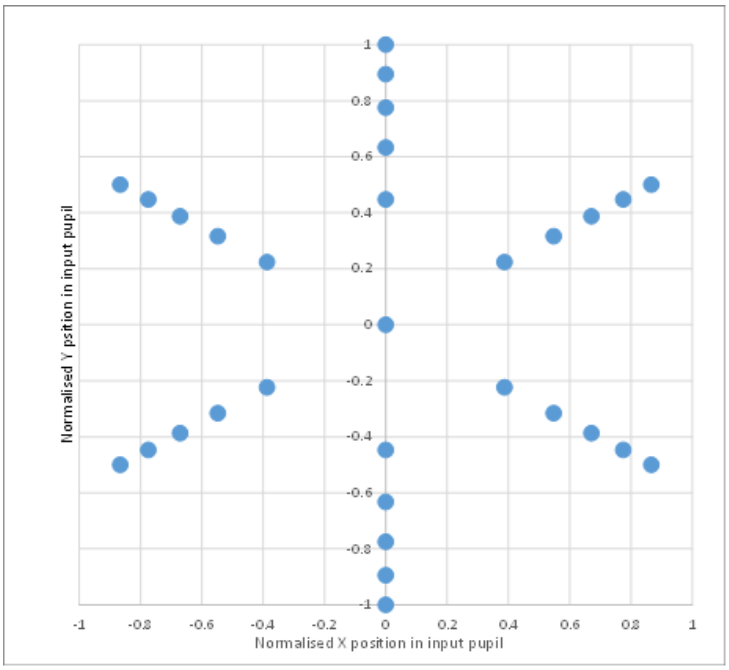

Figure 3-1: Pupil sampling map for TTL calculation

Figure 3-2 shows the reflective imaging system design for the science interferometers. The design meets all the requirements set out in 3.1, as well as all physical constraints imposed on the design. Figure 3-3 shows a 3D view of the reflective imaging system shown in Figure 3-2.

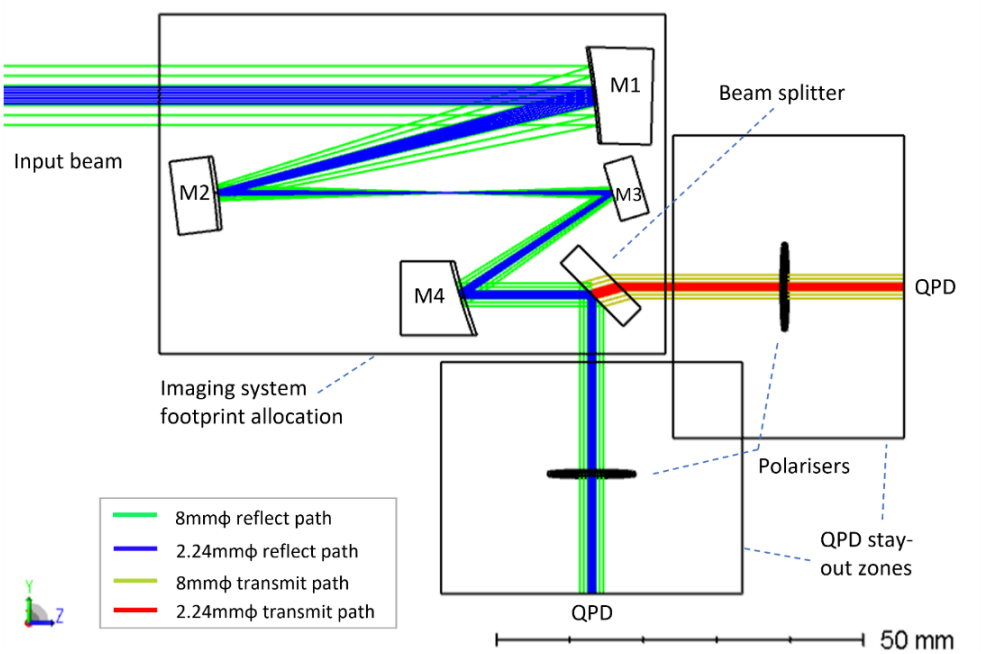

Figure 3-2: Reflective imaging system design for the science interferometer

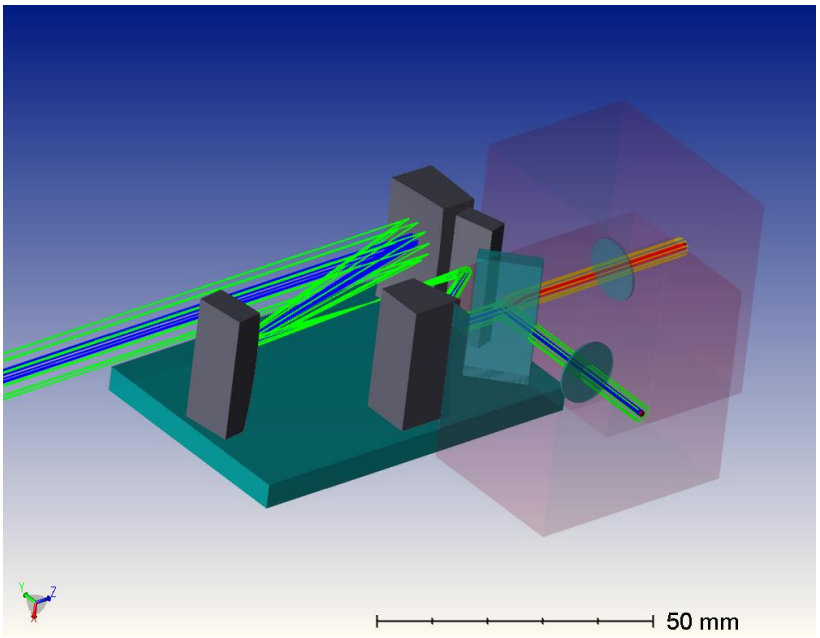

Figure 3-3: Reflective imaging system design for the science interferometer

3.3 Performance

The nominal TTL performance of this imaging system design is shown in Figure 3-4. This is well below the requirement of <13 µm/rad but is not considering tolerances. The nominal RMS WFE performance is 0.2 nm RMS over the 2.24 mm entrance pupil.

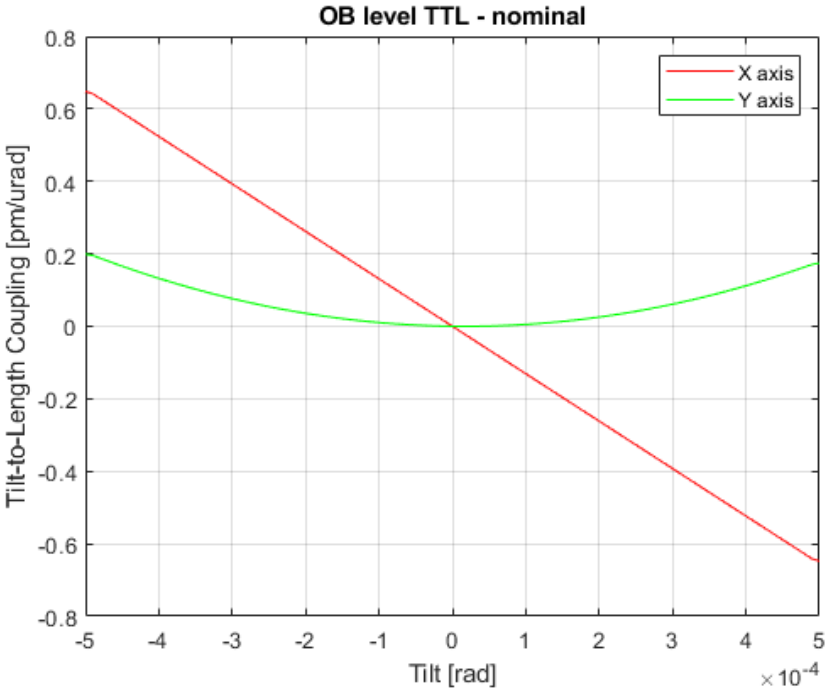

Figure 3-4: Nominal TTL performance of the science interferometer imaging system.

To give a more representative performance analysis, a tolerance analysis was completed. The set of tolerances used are shown in Table 3-1. These tolerances are a combination of manufacture and alignment tolerances, but are expected to be achievable.

Optic	dX – in plane / µm	dY – out of plane / µm	dZ / µm	rX – tilt out of plane / °	rY – tilt in plane / °	rZ – clocking about parent axis / °	Radius of curvature / %	Conic
M1	±25	±25	±25	±2.78E-3	±2.78E-3	±0.07	±1	±0.05
M2	±25	±25	±25	±2.78E-3	±2.78E-3	-	±1	-
M3	±25	±25	±25	±2.78E-3	±2.78E-3	-	-	-
M4	±25	±25	±25	±2.78E-3	±2.78E-3	±0.05	±0.5	±0.05

Table 3-1: Acceptable tolerances for the science interferometer imaging system.

This tolerance analysis was carried out as a 'worse case' alignment, whereby each individual optic was placed according to the tolerances in Table 3-1, with no sequential alignment. In practice, there is the possibility that successive optics can be aligned to compensate for some of the tolerances of previous optics, but this has not been considered for this tolerance analysis.

Figure *3-5*, Figure *3-6*, Figure *3-7* and Figure *3-8* show the results of a Monte Carlo analysis, consisting of 2,000 Monte Carlo runs. For these tolerances there is a 100% probability that the magnification error will be with the required ±0.02. There is a 95% probability that the chief ray vertical coordinate relative to the nominal QPD centre will be within ± 50 µm, which is the target in order to keep the beam within the adjustment range of the QPD. There is a 100% probability that the RMS WFE will be less than λ/38, which is well below the requirement of < λ/20. The difference in RMS WFE for off-axis beams is negligible. Finally, there is a 99% probability that the TTL is less than the requirement of <13 µm/rad.

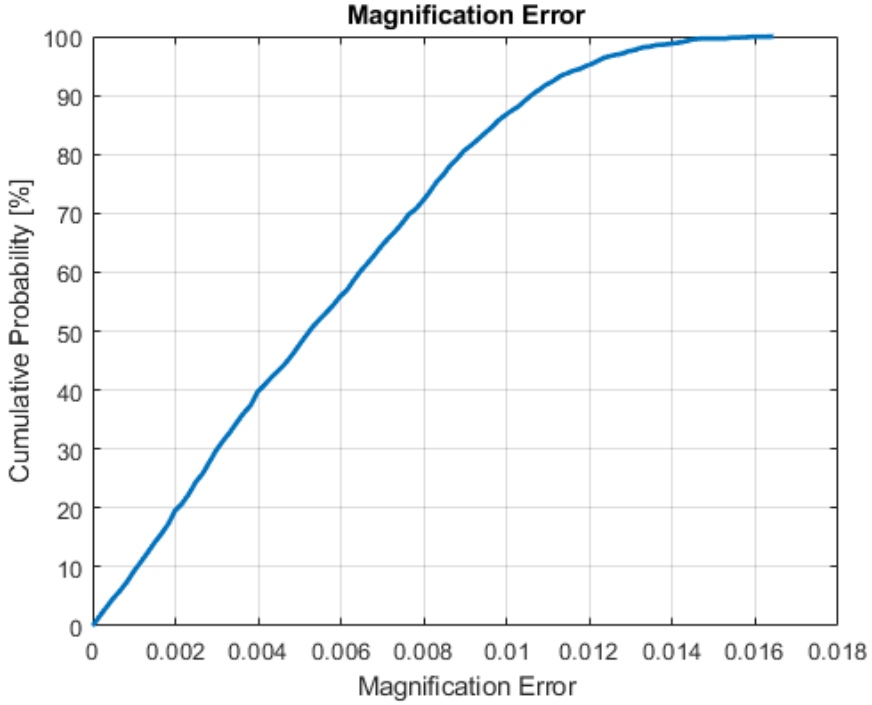

Figure 3-5: Cumulative probability of the magnification error of the toleranced imaging system design.

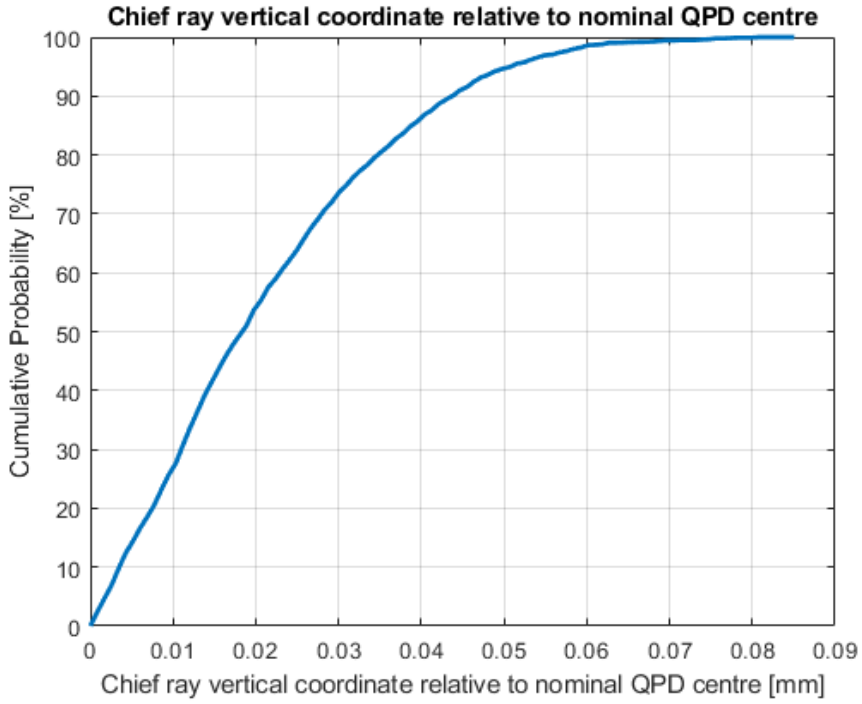

Figure 3-6: Cumulative probability of the chief ray coordinate error of the toleranced imaging system design.

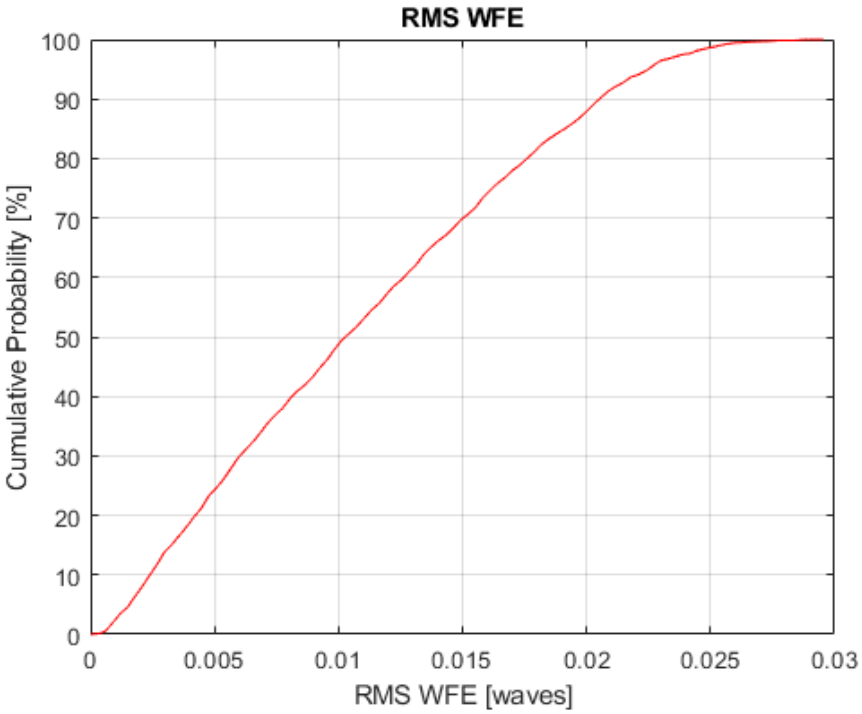

Figure 3-7: Cumulative probability of the RMS wavefront error of the toleranced imaging system design.

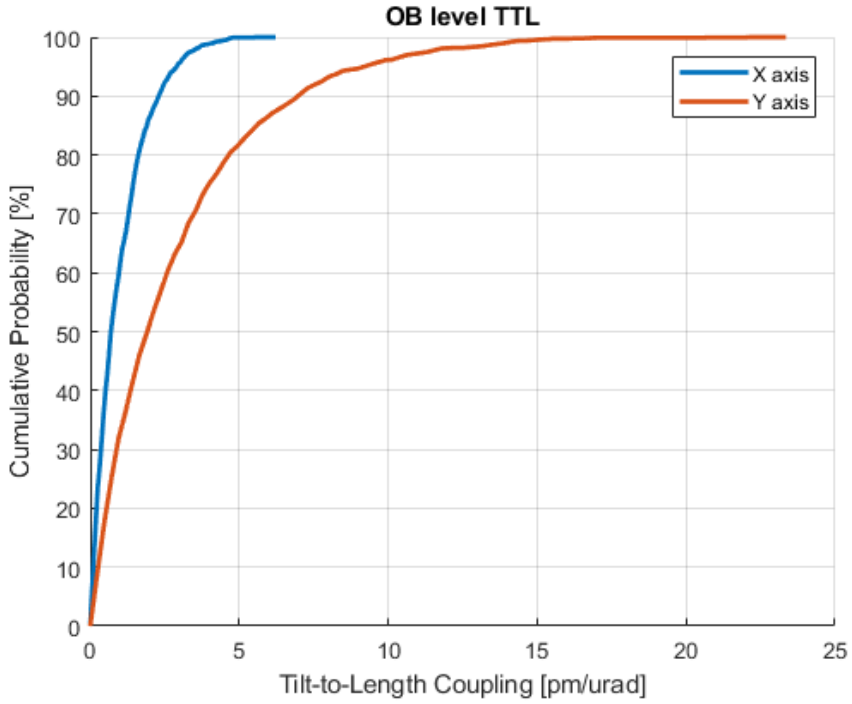

Figure 3-8: Cumulative probability of the TTL of the toleranced imaging system design.

4. STRAY LIGHT

Stray light poses a serious risk to the performance of LISA. Should stray light reach the QPDs on the optical bench, this is not inherently a problem for LISA. However should the stray light have a phase instability, then noise is directly imparted to the interferometric signal given changes in phase is the exact signature of a gravitational wave passing through the LISA constellation. Stray light can originate in numerous different ways and can reflect off both optical bench and non-optical bench structures. This makes it possible that phase instability can be imparted to the stray light - if the light interacts with an unstable / jittering structure somewhere on the spacecraft. In order to mitigate this risk to LISA, the mechanisms of stray light production must be understood. The key mechanisms being: ghost beams generated in the high-power Tx path, stray light generated by surface roughness of optics and stray light generated by particulate contamination on the surface of optics.

Given the knowledge of the precise optical bench layout and optical prescriptions, the location and direction of ghost beams are easily predetermined. The expected power of ghost beams can be well known too, as this depends on the efficiency of coatings and knowledge of the laser beam power. The Tx beam is the highest power beam on the optical bench and as such generates the most powerful ghost beams. As shown in Figure 2-1 and Figure 2-2, there are many planar mirrors on the optical bench used to direct the numerous laser beams. The coating on these mirrors are >99.9% reflective, meaning a small amount of light is transmitted i.e. a ghost beam. This light can then either reflect or transmit again at the back surface of the optic. The thickness of these planar mirrors are set such that in the case of a ghost beam reflection off the back surface, the ghost beam cannot pose a risk of re-entering the nominal Tx path. In the case of the ghost beam transmitting through the back surface of the planar optic, then beam dumps have been designed to suppress the ghost beam to negligible power levels.

The design of the optical bench beam dumps is shown in Figure *4-1* and Figure *4-2*. The incident beam is shown in Figure *4-1* as a red chief ray and two black-dashed rays which trace the beam radius out to negligible power levels. The beam dump consists of two angled glass plates that reflect the beam many times between them. At each reflection a small portion of the beam power is transmitted into the glass where the light is absorbed. Schott BG18 was chosen as the glass type as it absorbs highly at 1064nm. The angles and dimensions of the glass plates have been optimized in order to dump the light

as efficiently as possible whilst minimizing the footprint of the beam dump on the optical bench. For a 1W incident ghost beam, the power of the beam leaving the beam dump is <1pico-Watt, demonstrating the suppression power of the beam dump.

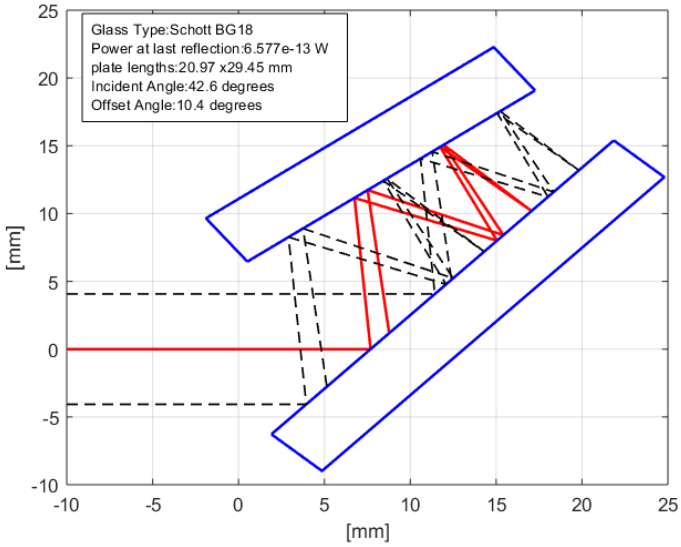

Figure 4-1: Glass plate beam dump design

Figure 4-2 shows the complete optomechanical model of the beam dump. The glass plates are bonded to a vertical wall of titanium. Three small feet can be seen on the bottom side of the beam dump. These are carefully designed to supply a strong enough bonding area to the optical bench, whilst minimizing the transfer of heat from the beam dump to the optical bench.

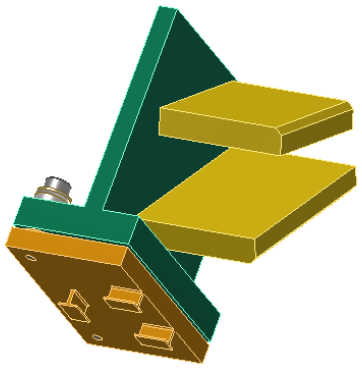

Figure 4-2: Glass plate beam dump design – optomechanical model

The beam dump performance is expected to be limited by stray light due to surface roughness and contamination, which is much harder much harder to model and control than ghost beams. Surface roughness and contamination will scatter light out of the beam path, weighted towards the specular directions. This light can reflect or scatter off other structures and get back onto nominal beam paths. This poses a risk if the structure that the scattered light reflects off is unstable / jittering at time scales in the LISA frequency measurement band. More of a risk however, is scattered light which travels straight back down the incident beam path, of within a narrow cone angle of approximately +/-2mrad. This stray light poses a serious risk of making its way to the interferometers, which can be problematic if the beam dump itself is thermally unstable or jittering.

To model the surface roughness of the glass and the resulting stray light the software FRED was used. The Bi-Directional Scatter Distribution Function (BSDF) i.e. the angle dependence of scattered light, can be modelled using three parameters 'A', 'B' and 'g'[10]. These parameters are not directly linked to the description of surface roughness, but instead are simply equation parameters used to produce a BSDF that matches empirically measured BSDF profiles. Equation *4-1* shows the functional form of the BSDF used to model the scatter due to surface roughness

$$BSDF\big(\sin(\theta_{scatter}) - \sin(\theta_{specular})\big) = \frac{A}{B + (\sin(\theta_{scatter}) - \sin(\theta_{specular}))^{g}} \qquad [sr^{-1}]$$

Equation 4-1: The Bi-Directional Scatter Distribution Function (BSDF)

Modelling contamination is somewhat harder than modelling surface roughness. This is inherent in the fact that particle distribution profiles are not easily predictable i.e. particle size, count, composition, distribution and dependence on time. A common approximation of these variables is made using MIL-STD-1246. Again FRED can be used to model this stray light, dependent on the particle distribution profile described by MIL-STD-1246.

Figure *4-3* shows the scattered light levels leaving the beam dump in the direction of the incident beam, +/-2mrad. The 'slope' value of 0.926 is stated and is the default value for MIL-STD-1246. The slope parameter (ranging from 0 to 1) describes the balance of 'large' to 'small' particles within the particle distribution. A value of 0.926 is expected to be typical for most contamination profiles of optics - as stated by MIL-STD-1246. The plot shows that stray light due to contamination is dominant over stray light due to surface roughness. 1nm to 5nm RMS surface roughness is an achievable range for polishing of flat optics. CL200 is stated as 'clean' in MIL-STD-1246, whilst CL600 is described as having 'visible' particles across the surface of the optic and is the typical cleanliness level expected for launched space missions.

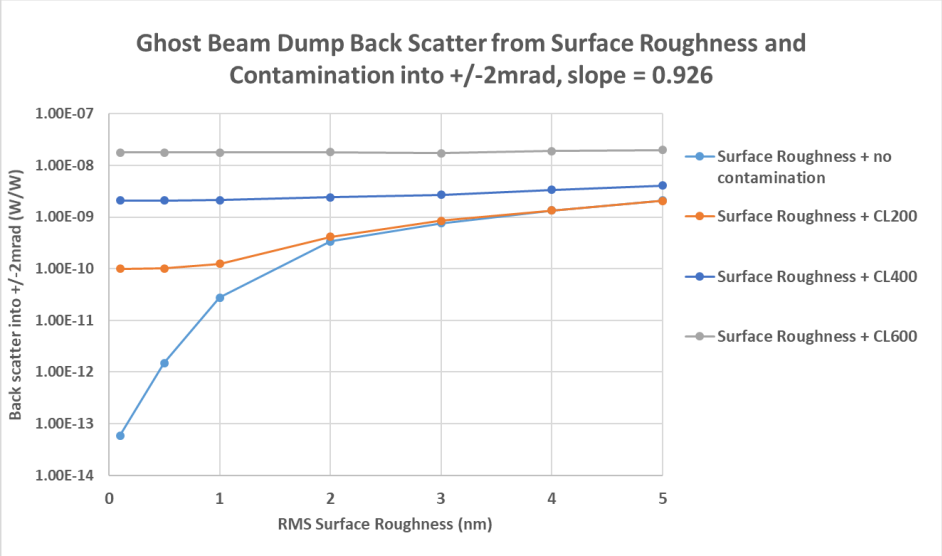

Figure 4-3: Scattered light due to surface roughness and contamination leaving the beam dump in the direction of the incident beam, +/-2mrad

To assess whether these stray light levels are acceptable or not, the performance impact of stray light into the science interferometer must be calculated. The beam dump behind PBS1 has a direct coupling path to the Science interferometer as it backscatters directly into the Rx path, shown in Figure *4-4*. The following calculation is considering just the beam dump behind PBS1 as this beam dump will see the highest amount of power and so poses the largest risk of stray light. Note, Figure *4-4* shows an earlier version of the optical bench layout, but the below analysis is still valid given the optical similarities between the old and new layout.

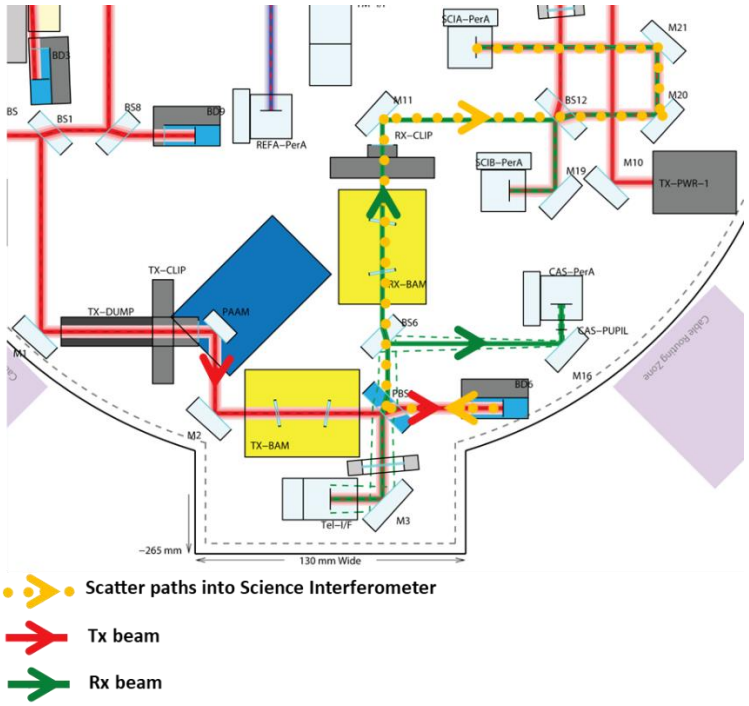

Figure 4-4: A significant stray light path from a beam dump to the science interferometer. Note this shows an earlier version of the optical bench layout

The longitudinal stability of the component from which the stray light originates (Δx_{SL}) must first of all be determined. Here, we assume that the principal perturbation is temperature noise, and therefore this is estimated simply as the product of the optic and/or mount thickness, the mount CTE and the optical bench thermal stability. Note, this CTE model is simple, but conservative. From there, Equation 4-2 is used to determine the coupling of stray light phase noise to interferometer phase noise

$$\delta x_{sci} = \epsilon_{bal} \cdot \epsilon_{mode} \cdot \epsilon_{pol} \sqrt{\frac{P_{SL}}{P_{TX/SCI}}} \Delta x_{SL}$$

Equation 4-2: Path length noise in the interferometer. Parameters are described in Table 4-1:

The Equation 4-2 parameter definitions are stated in Table *4-1*.

Parameter	Value	Description
δx_{sci} (m/√Hz)	Determined according to Equation 4-2	Introduced path length noise due to stray light
ϵ_{bal}	0.15	Suppression factor for balanced detection in the science interferometer
ϵ_{mode}	0.5	Model overlap between the scattered light and the TX beam at the science interferometer (conservative)
ϵ_{pol}	0.5	Suppression due to polarisation mismatch between the backscatter and the PBS (worst case)

P_{SL} (W)	From stray light analysis above	Stray light power
$P_{TX/SCI}$ (W)	6.15E-03	Worst case for Tx power at SCI-IFO
Δx_{SL} (m/√Hz)	Determined for each optic using below parameters and optical bench thermal stability	Phase stability of the scattered light
CTE Ti (/K)	9.00E-06	
Beam dump thickness (m)	0.05	

Table 4-1: Parameters used in the path length noise equation (Equation 4-2)

Figure *4-5* shows the stray light induced interferometer noise, with respect to the optical bench thermal stability – ranging from 1e-7 k/√Hz to 1e-2 k/√Hz. This is calculated for a beam dump at 3nm RMS surface roughness and CL600 cleanliness level. The requirement for optical bench thermal stability is 10 μK/√Hz. At this value, the path length noise induced by the beam dump behind PBS1 into the science interferometer is 3e-16 m/√Hz, i.e. completely negligible. Another result we can extract is that in order to keep the path length noise contribution to be less than 0.1 pm/√Hz (which would still be a negligible contribution in the measurement budget), the beam dump must have a thermal stability of 3 mK/√Hz, i.e. over 2 orders of magnitude higher than the optical bench temperature stability requirement.

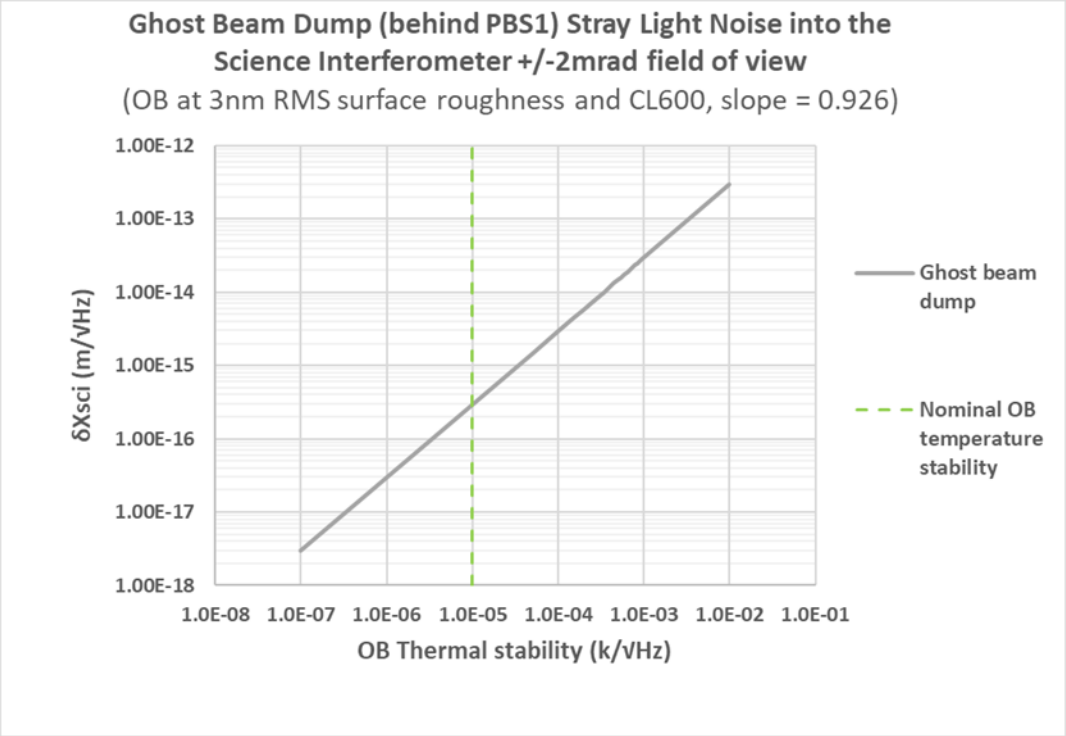

Figure 4-5: Stray light induced interferometer noise, with respect to the optical bench thermal stability. This is for the particular beam dump sat behind PBS1. 'OB' = Optical Bench.

This stray light analysis tells us that for the most stray light producing beam dump, the stray light levels are not going to cause any noticeable noise in the interferometric signal. However, this is for only one stray light path and it remains to be determined if there are other more problematic paths. For example, the thermal stability of the structure surrounding the optical bench is unknown and could impart significant levels of interferometer noise, should stray light interact with it. It is therefore an on-going process to identify these paths and to mitigate the production of stray light in the first place. Polishing optics to a high standard clearly helps reduce stray light. However, the reduction of contamination is expected to be the most beneficial means of reducing stray light on the LISA optical bench.

5. CONCLUSION

This paper provides an overview of the LISA optical bench, including a functional description and detailing of the many subsystems. The optical bench is only part of LISA and there are many other systems to understand in order to grasp how LISA functions as a whole. Sections 3 and 4 go into detail on the engineering challenges faced by TTL and stray light mitigation respectively.

Imaging systems are a key TTL mitigation and a working design was demonstrated. The design was shown to meet all requirements under realistic tolerances and alignment to a high confidence level. The space constraints on the imaging systems were also met, enabling a full optical bench layout that fits into the baseplate dimensions.

A detailed stray light analysis was shown for the optical bench beam dumps. These beam dumps are critical for mitigation of stray light. It has been demonstrated that the current beam dump design can successfully suppress stray light to negligible levels in terms of interferometric noise.

REFERENCES

[1] Abbott, B. P & Abbott, R. & Abbott, Thomas & Abernathy, Matthew & Acernese, Fausto & Ackley, K. & Adams, C. & Adams, Teneisha & Addesso, Paolo & Adhikari, R. X & Adya, Vaishali & Affeldt, C. & Agathos, M. & Agatsuma, Kazuhiro & Aggarwal, Nishu & Aguiar, Odylio & Aiello, L. & Ain, Anirban & Ajith, P. & Zweizig, John. (2016). Observation of Gravitational Waves from a Binary Black Hole Merger. Physical Review Letters. 116. 10.1103/PhysRevLett.116.061102.

[2] Amaro-Seoane, P., Audley, H., Babak, S., Baker, J., Barausse, E., Bender, P., Berti, E., Binetruy, P., Born, M., Bortoluzzi, D. and Camp, J., 2017. Laser interferometer space antenna. *arXiv preprint arXiv:1702.00786*.

[3] Petiteau, A., 2021, June. LISA: Observing Universe with Gravitational Waves from space. In *International Conference on Space Optics—ICSO 2020* (Vol. 11852, pp. 30-66). SPIE.

[4] Tinto, M., Dhurandhar, S.V. Time-delay interferometry. Living Rev Relativ 24, 1 (2021).

[5] D I Robertson et al 2013 Class. Quantum Grav. 30 085006.

[6] van Veggel, Anna-Maria A. and Killow, Christian J.. "Hydroxide catalysis bonding for astronomical instruments" Advanced Optical Technologies, vol. 3, no. 3, 2014, pp. 293-307.

[7] David I. Robertson, Ewan D Fitzsimons, Christian J. Killow, Michael Perreur-Lloyd, and Henry Ward, "Automated precision alignment of optical components for hydroxide catalysis bonding," Opt. Express 26, 28323-28334 (2018).

[8] Ewan D. Fitzsimons, Johanna Bogenstahl, James Hough, Christian J. Killow, Michael Perreur-Lloyd, David I. Robertson, and Henry Ward, "Precision absolute positional measurement of laser beams," Appl. Opt. 52, 2527-2530 (2013).

[9] Chwalla, M., et al. "Optical suppression of tilt-to-length coupling in the LISA long-arm interferometer." *Physical Review Applied* 14.1 (2020): 014030.

[10] Pfisterer, R. N. "Approximated Scatter Models for Stray Light" - https://photonengr.com/wp-content/uploads/2014/10/ApproximatedScatter1.pdf.